Proportionate Normalized Least Mean M-estimate Controlled Shunt Converter for Load Balancing in Distribution Grid

Jayant Sharma, *Member*, *IEEE*, Chinnayan Karuppaiyah Sundarabalan, *Senior Member*, *IEEE*, and Chelladurai Balasundar, *Member*, *IEEE*

***Abstract*—Nonlinear loads and power electronics components inject harmonics into the connected power system, which affects the power quality of the system. Harmonic suppression, reactive power compensation, and load balancing can be accomplished with the use of shunt converters. This paper proposes a proportionate normalized least mean M-estimate controlled shunt converter to separate the distorted load current's active and reactive components. The control algorithm introduces the M-estimate based cost function, which helps remove the impact of impulsive noise on weight update. The shunt converter is designed to balance load, compensate for reactive power, and reduce harmonics in the distribution system. To determine the proposed control algorithm's robustness, the system is tested under a variety of linear and nonlinear load scenarios. The proposed control is compared to four existing control strategies to demonstrate its effectiveness in evaluating the components of load current. Experimental analysis is carried out through real-time simulation analysis using the dSPACE 1202 processor. The proposed system is validated to comply with the IEEE-519 standards.**

***Index Terms*—Adaptive control, harmonics, PNLMM, power quality, shunt converter.**

NOMENCLATURE

A. Abbreviations

DSTATCOM	distribution static compensator
PCC	point of common coupling
PFC	power factor correction
VSC	voltage source converter
LMS	least mean square
LLMLF	leaky least mean logarithmic fourth
PNLMF	proportionate-normalized least mean fourth
RLM	recursive least M-estimate
RLS	recursive least square
LMM	least mean M-estimate
PNLMM	proportionate normalized least mean M-estimate
PQ	power quality
LMF	least mean fourth
PI	proportional integral
RTW	real-time workshop
THD	total harmonic distortion

B. Variables

L_s	source inductance
R_s	source resistance
$u_{p,a,b,c}$	active unit templates
$u_{p,a,b,c}$	reactive unit templates
$w_{q,a,b,c}$	fundamental reactive weights
$v_{s,a,b,c}$	PCC phase voltages
v_{dc}	DC link voltage
v_{dc}^*	reference DC link voltage
$Z_{L,a,b,c}$	impedances of linear load
$e_{p,a,b,c}$	active error currents
i_{sn}	supply-side neutral current
i_{cn}	converter neutral current
w_{pavg}	average active weight
$i_{L,a,b,c}$	load currents
w_{cp}	output of DC link PI controller
$w_{p,a,b,c}$	fundamental active weights
$v_{m,a,b,c}$	internal phase voltages
V_t	PCC voltage magnitude

Received: February 21, 2024
Accepted: August 23, 2024
Published Online: January 1, 2025

Jayant Sharma and Chinnayan Karuppaiyah Sundarabalan (corresponding author) are with the School of Electrical and Electronics Engineering, SASTRA Deemed University, Thanjavur 613401, India (e-mail: sharmajayant01234@gmail. com; ckseee@yahoo.com).

Chelladurai Balasundar is with the Department of EEE, Thiagarajar College of Engineering, Madurai, Tamilnadu 625015, India (sun14061990@gmail.com).

DOI: 10.23919/PCMP.2023.000144

i_{Ln}	load-side neutral current
$e_{\mathrm{q,a,b,c}}$	reactive error currents
ε	regularization parameter
α, β	small positive constants
ξ	threshold parameter
$\psi(\cdot)$	score function
σ_{e}	robust estimator
λ_{a}	forgetting factor
c_1	finite sample correction
$\mathrm{med}(\cdot)$	median operator
N_{w}	estimation window
$i_{\mathrm{s,a,b,c}}$	source currents
w_{qavg}	average reactive weight
w_{sp}	reference active weight
w_{sq}	reference reactive weight
$i_{\mathrm{C,a,b,c}}$	converter currents
G_{pa}	intermediate signal of PNLMM
$i^*_{\mathrm{p,a,b,c}}$	active reference currents
$i^*_{\mathrm{q,a,b,c}}$	reactive reference currents
$i^*_{\mathrm{s,a,b,c}}$	reference source currents

I. Introduction

In recent years, the capability of the distribution systems to deliver sinusoidal current and voltage has been limited by increasing utilization of power electronics-based load and nonlinear load such as phase-controlled rectifiers, solid-state drives or arc furnaces, which inject harmonic currents into the power system [1], [2]. These harmonics can cause harm to motor loads, producing excessive heating and pulsating torques that can significantly reduce motor life [3].

Use of passive and active power filters can help alleviate these PQ issues [4]. However, active filters are critical in effective mitigation of power quality issues in distribution systems [5], primarily because of their significant advantages over passive filters [6]. A shunt converter, namely, DSTATCOM, is an active filter used not only for injecting reactive power at the PCC and suppressing harmonics, but also for load balancing in zero voltage regulation and PFC modes [7]. In [8] and [9], load balancing and power quality mitigation techniques using DSTATCOM are discussed, while in [10], a single-loop flatness-based controller is used to control the currents of the VSC. A new control approach for U-Cell converter based medium voltage DSTATCOM is discussed in [11], and in [12], a collaborative control method is used for a hybrid compensator consisting of DSTATCOM and a static VAR compensator. Reference [13] implements Lyapunov based harmonic compensation, which provides low implementation complexity with effective source current harmonic suppression for EV charging applications. In [14], a fuzzy system and synchronous reference theory controlled DSTATCOM is implemented to improve PQ in wind energy system. The efficacy of the DSTATCOM has been assessed for compensating reactive power in a standalone solar power system with a capacity of 100 kW [15].

DSTATCOM offers control flexibility through the utilization of either time-domain-based or frequency-domain-based controls. Frequency-domain techniques involve heavy calculations and slow response. Therefore, they are rarely used in the control of custom power devices like unified power quality conditioner, DSTATCOM and dynamic voltage restorer. Adaptive control algorithms can be used to overcome the difficulty of the slow convergence rate and computational complexity of conventional algorithms. Reference [16] evaluates the performance of the adaptive LMS algorithm for harmonic extraction in three-phase systems.

DSTATCOM control has been accomplished using the Adaline-LMS adaptive algorithm [17], LLMLF technique [18], generalized maximum versoria criterion filter [19], and PNLMF [20]. In [21], an adaptive observer-based approach is used for the DSTATCOM compensator to optimize controller parameters in a rooftop PV system, while interval type-II fuzzy logic is implemented for the shunt converter control in electric vehicle charging stations in [22], [23]. Sliding mode control is utilized in DSTATCOM control in order to reduce changes in DC link capacitor voltage in [24], while backstepping control is proposed in [25] for multilevel DSTATCOM control. Moreover, various DSTATCOM based neutral current compensation techniques have been studied. In [26], the Euclidean direction search technique is implemented for the neutral current compensation using DSTATCOM, and in [27], a new virtual Y-TCR based technique is proposed for the compensation of neutral current under the unbalanced linear load condition. A capacitive-coupling winding tap injection DSTATCOM is proposed in [28] to alleviate PQ and compensate for neutral current under the unbalanced linear load condition in distribution system. Reference [29] presents the RLM approach to mitigate the detrimental effects of large estimation errors produced by impulses on filter weights. When impulses alter the input and desired signals, it is noted in [29] that the RLM method outperforms the conventional RLS and normalized RLS algorithms. The robust M-estimate function is used to examine the effectiveness of LMM in [30], whereas the score functions, known for effectively suppressing impulse noise signals, have been investigated as M-estimate functions [31].

This paper uses the PNLMM technique in DSTATCOM control for the filtration of fundamental reactive and active load currents. These filtered parts of the load current are utilized to determine the reference source current. The PNLMM algorithm employs an M-estimate cost function to compute reference source current, mitigating substantial estimation errors induced

by impulses. The score function is utilized in the PNLMM-based control algorithm. The proposed PNLMM control algorithm is compared to four existing adaptive algorithms, including Adaline LMS, LLMLF, PNLMF and RLM, in terms of dynamic performance. This work offers noteworthy contributions in the following aspects:

1) An improved M estimation cost function based algorithm is used to filter positive sequence part of polluted and unbalanced load current.

2) Effective power quality improvement using the PNLMM control approach by lowering the harmonic content of the load current created by nonlinear loads.

3) Effective compensation of unbalanced load current using PNLMM controlled four-leg distribution static compensator.

4) Dynamic and steady-state analysis of PNLMM control algorithm with Adaline LMS, LLMLF, PNLMF and RLM control algorithms.

5) Empirical validation of the proposed work using dSPACE based real-time analysis.

The remaindar of the paper is organized as follows. Section II provides a detailed modelling of the four-leg DSTATCOM, along with the incorporation of three-phase linear/nonlinear loads and a description of the proposed control method. The results and their corresponding discussions are encapsulated in Section III. Finally, Section IV draws the conclusions from this work.

II. System Description and Control Algorithm

An DSTATCOM is tied to a three-phase four-wire supply with source inductance L_s and source resistance R_s in the system configuration shown in Fig. 1. A four-legged VSC, a DC link capacitor, and interfacing inductors are included in the DSTATCOM. The system features linear loads, and a three-phase diode bridge rectifier is connected to a balanced three-phase supply. As discussed earlier, a nonlinear load draws non-sinusoidal current from a balanced supply even if the supply voltage is purely sinusoidal. Compensating current injected by VSC at the PCC eliminates the non-sinusoidal current and supply reactive power demand of the load connected at the PCC. VSC switching produces high-frequency noise, which is reduced by a ripple filter (a series connection of C_f and R_f). The presented PNLMM control technique for reference current extraction is depicted in Fig. 2. This approach is employed to estimate both the active and reactive components of the load current.

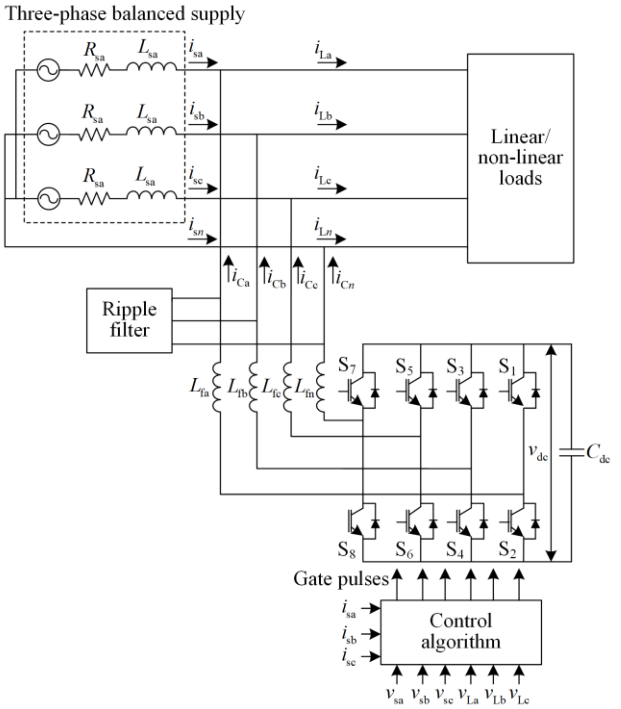

Fig. 1. System under study.

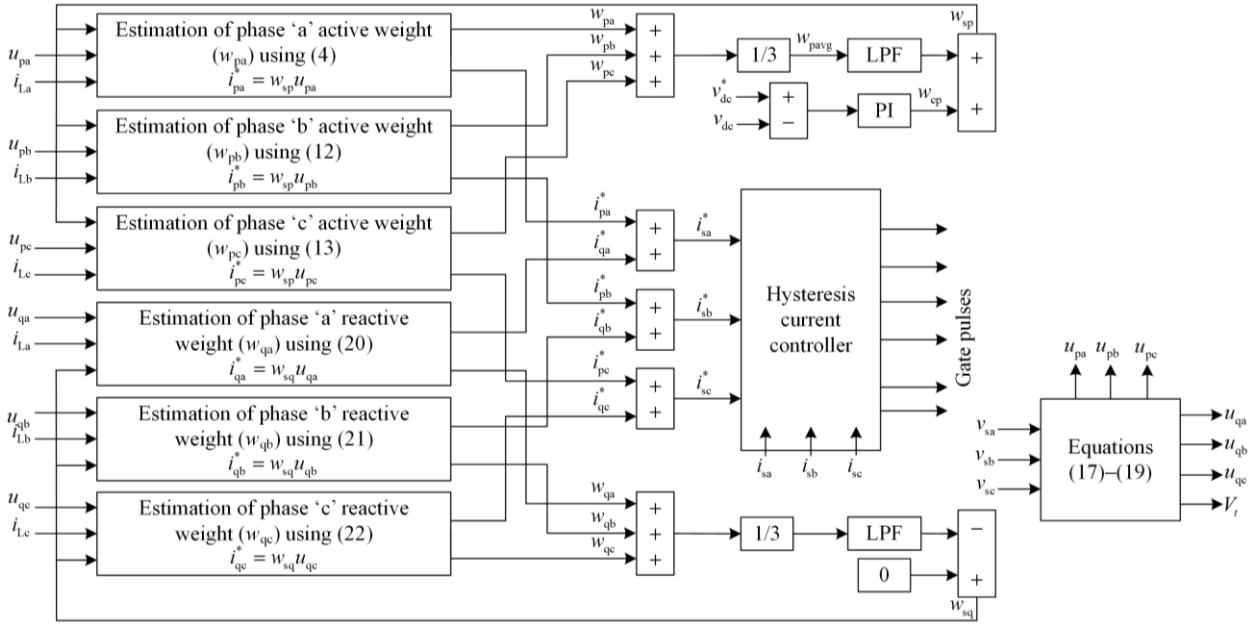

Fig. 2. Structure of PNLMM adaptive control algorithm.

The Simpower systems toolbox in Matlab/Simulink is used for the simulation investigation, and then experimentation of the proposed approach is conducted by real-time simulation analysis. The mathematical modelling of the PNLMM algorithm is derived below and is shown in Fig. 2.

A. Reference Active Current Calculation

The calculation of u_{pa}, u_{pb} and u_{pc} is as follows:

$$u_{\mathrm{pa}}=\frac{v_{\mathrm{sa}}}{V_t},u_{\mathrm{pb}}=\frac{v_{\mathrm{sb}}}{V_t},u_{\mathrm{pc}}=\frac{v_{\mathrm{sc}}}{V_t} \tag{1}$$

where V_t is the PCC voltage magnitude, given as:

$$V_t=\sqrt{\frac{2(v_{\mathrm{sa}}^2+v_{\mathrm{sb}}^2+v_{\mathrm{sc}}^2)}{3}} \tag{2}$$

The voltage across the capacitor connected to the DC side of the VSC is represented as v_{dc}. The DC voltage v_{dc} is monitored and compared to the reference voltage v_{dc}^*, while the error is passed to a PI controller. Phase a load current is denoted by i_{La} and phase a in-phase unit template is u_{pa}.

$$e_{\mathrm{pa}}(n)=i_{\mathrm{La}}(n)-u_{\mathrm{pa}}(n)w_{\mathrm{pa}}(n) \tag{3}$$

where $w_{\mathrm{pa}}(n)$ is the weight vector at the nth interval. The weight update equation of the PNLMM algorithm for reference current estimation of the fundamental load component of phase a is given as [31]:

$$w_{\mathrm{pa}}(n+1)=\mu\psi(e_{\mathrm{pa}}(n))u_{\mathrm{pa}}(n)P_{\mathrm{pa}}(n)+w_{\mathrm{pa}}(n) \tag{4}$$

where

$$P_{\mathrm{pa}}(n)=\frac{G_{\mathrm{pa}}(n)}{u_{\mathrm{pa}}^T G_{\mathrm{pa}}(n)u_{\mathrm{pa}}(n)+\varepsilon} \tag{5}$$

where ε is a small regularization parameter ($0.001<\varepsilon<0.01$), which is taken into account in order to avoid the risk of instability in this method. The typical number is between 0 and 2.

$G_{\mathrm{pa}}(n)$ is given as [30]:

$$G_{\mathrm{pa}}(n)=\frac{\left|w_{\mathrm{pa}}(n)\right|}{\sum_{i=0}^{M-1}\left|w_{\mathrm{pa}}(n)\right|+\alpha}+\beta \tag{6}$$

where α and β are small positive constants so that $G_{\mathrm{pa}}(n)$ remains stable. In (4), $\psi(e_{\mathrm{pa}}(n))$ is employed. For clipping of transient variations of error, score function, as shown in Fig. 3, is utilized. $\psi(e_{\mathrm{pa}}(n))$ is given as:

$$\psi(e_{\mathrm{pa}}(n))=\begin{cases}e_{\mathrm{pa}}(n), \left|e_{\mathrm{pa}}(n)\right|<\xi\\ 0, \left|e_{\mathrm{pa}}(n)\right|\geq\xi\end{cases} \tag{7}$$

When the absolute value of $e_{\mathrm{pa}}(n)$ is less than ξ, $\psi(e_{\mathrm{pa}}(n))$ simplifies to $e_{\mathrm{pa}}(n)$, resulting in the transformation of the PNLMM algorithm into the PNLMS algorithm. Conversely, if $\left|e_{\mathrm{pa}}(n)\right|$ exceeds ξ, $\psi(e_{\mathrm{pa}}(n))$ approaches zero.

$$\xi=2.576\sigma_e(n) \tag{8}$$

where $\sigma_{\mathrm{e}}(n)$ is the robust estimator, given as:

$$\sigma_{\mathrm{e}}^2(n)=\lambda_\sigma\sigma_{\mathrm{e}}^2(n-1)+c_1(1-\lambda_\sigma)med(A_{\mathrm{e}}(n)) \tag{9}$$

$$c_1=1.483\left(1+\frac{5}{(N_{\mathrm{W}}-1)}\right) \tag{10}$$

where λ_σ is the forgetting factor.

The value of $A_{\mathrm{e}}(n)$ is:

$$A_{\mathrm{e}}(n)=\left[e^2(n),e^2(n-1),\cdots,e^2(n-N_{\mathrm{W}}+1)\right] \tag{11}$$

For reference current estimation of the fundamental load constituents of phases b and c, the PNLMM control algorithm's weight are updated as:

$$w_{\mathrm{pb}}(n+1)=\mu\psi(e_{\mathrm{pb}}(n))u_{\mathrm{pb}}(n)P_{\mathrm{pb}}(n)+w_{\mathrm{pb}}(n) \tag{12}$$

$$w_{\mathrm{pc}}(n+1)=\mu\psi(e_{\mathrm{pc}}(n))u_{\mathrm{pc}}(n)P_{\mathrm{pc}}(n)+w_{\mathrm{pc}}(n) \tag{13}$$

The weights determined for each phase in (4), (12), and (13) are used to generate the average active weight value w_{pavg}:

$$w_{\mathrm{pavg}}=(w_{\mathrm{pa}}+w_{\mathrm{pb}}+w_{\mathrm{pc}})/3 \tag{14}$$

To calculate the reference active weight w_{sp}, w_{pavg} is combined with w_{cp}, i.e.:

$$w_{\mathrm{sp}}=w_{\mathrm{pavg}}+w_{\mathrm{cp}} \tag{15}$$

The weight w_{sp} in (15) and in-phase templates (1) are multiplied to determine active reference current, given as:

$$i_{\mathrm{pa}}^*=w_{\mathrm{sp}}u_{\mathrm{pa}},i_{\mathrm{pb}}^*=w_{\mathrm{sp}}u_{\mathrm{pb}},i_{\mathrm{pc}}^*=w_{\mathrm{sp}}u_{\mathrm{pc}} \tag{16}$$

B. Reference Reactive Current Calculation

The determination of quadrature unit templates involves the utilization of in-phase unit templates (1):

$$u_{\mathrm{qa}}=\frac{(u_{\mathrm{pc}}-u_{\mathrm{pb}})}{\sqrt{3}} \tag{17}$$

$$u_{\mathrm{qb}}=\frac{\sqrt{3}u_{\mathrm{pa}}}{2}-\frac{(u_{\mathrm{pc}}-u_{\mathrm{pb}})}{2\sqrt{3}} \tag{18}$$

$$u_{\mathrm{qc}}=-\frac{\sqrt{3}u_{\mathrm{pa}}}{2}-\frac{(u_{\mathrm{pc}}-u_{\mathrm{pb}})}{2\sqrt{3}} \tag{19}$$

To align the voltage of V_t with V_{tr}, an additional PI controller is essential to reduce the difference between the two. This necessity arises due to impedance voltage

drops within the power network. The output of the PI controller is denoted as w_{cq}. The reactive weights (w_{qa}, w_{qb}, and w_{qc}) are determined as follows:

$$w_{qa}(n+1) = \mu\psi(e_{qa}(n))u_{qa}(n)P_{qa}(n) + w_{qa}(n) \quad (20)$$

$$w_{qb}(n+1) = \mu\psi(e_{qb}(n))u_{qb}(n)P_{qb}(n) + w_{qb}(n) \quad (21)$$

$$w_{qc}(n+1) = \mu\psi(e_{qc}(n))u_{qc}(n)P_{qc}(n) + w_{qc}(n) \quad (22)$$

The average reactive weight is calculated as:

$$w_{qavg} = (w_{qa} + w_{qb} + w_{qc})/3 \quad (23)$$

To determine the reference reactive weight (w_{sq}), w_{qavg} is subtracted from w_{cq} as:

$$w_{sq} = w_{cq} - w_{qavg} \quad (24)$$

$$i_{qa}^{*} = w_{sq}u_{qa}, i_{qb}^{*} = w_{sq}u_{qb}, i_{qc}^{*} = w_{sq}u_{qc} \quad (25)$$

Using (16) and (25), the three-phase reference source current are computed as follows:

$$i_{sa}^{*} = i_{qa}^{*} + i_{pa}^{*}, i_{sb}^{*} = i_{qb}^{*} + i_{pb}^{*}, i_{sc}^{*} = i_{qc}^{*} + i_{pc}^{*} \quad (26)$$

A comparison is made between the calculated reference source current and the measured source current. A PWM current controller receives the error created by the comparison, and then gating signals are generated by the PWM controller.

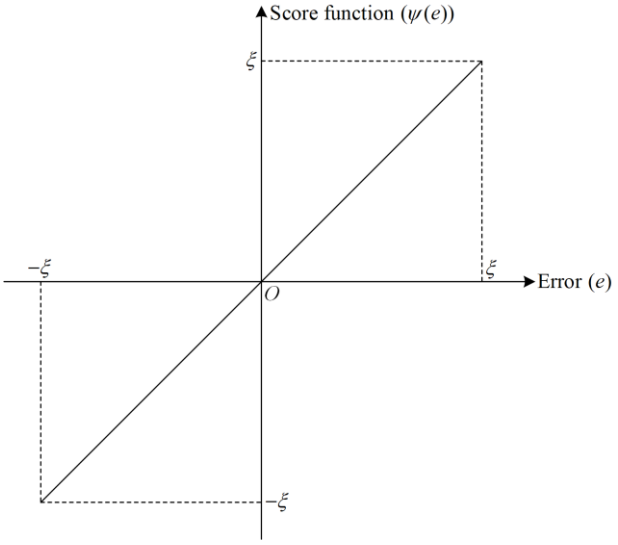

Fig. 3. Score function.

III. Results and Discussion

The efficacy of the proposed PNLMM control algorithm for DSTATCOM is validated and assessed through Matlab/Simulink. The DSTATCOM's performance is observed in load balancing mode and PFC mode, considering both balanced and unbalanced linear/nonlinear loading scenarios. Simulation design parameters are given in Table I.

TABLE I
Design Parameters

Parameters	Symbol	Design values
Grid voltage	V_{LL}	415 V (RMS)
Supply frequency	f (Hz)	50
Source resistance per phase	R_{sa} (Ω)	0.01
Source inductance per phase	L_{sa} (mH)	2
Switching frequency	f_{sw} (kHz)	10
Sampling time	T_s (μs)	50
Voltage of DC link	v_{dc} (V)	700
Interfacing inductor	L_f (mH)	10
Filter capacitor	C_r (μF)	5
Ripple filter resistor	R_r (Ω)	100
DC-link capacitor	C_{dc} (μF)	3000
Three-phase nonlinear load resistor	R_L (Ω)	61
Three-phase nonlinear load inductor	L_L (mH)	194
Linear load a-phase resistor	R_{La} (Ω)	40
Linear load a-phase inductor	L_{La} (mH)	65
Linear load b-phase resistor	R_{Lb} (Ω)	50
Linear load b-phase inductor	L_{Lb}	85
Linear load c-phase resistor	R_{Lc} (Ω)	110
Linear load c-phase inductor	L_{Lc} (mH)	420
Optimised gains of DC bus PI controller	K_{id}, K_{pd}	1.1397, 0.037834
PNLMM algorithm parameters	μ	0.2
	N_W	8
	β	0.1
	ε	0.2
	α	0.2
	σ_y	0.98

A. Performance of the Distribution Static Compensator in PFC Mode Under Nonlinear Loading

A uncontrolled three-phase converter-based nonlinear load is connected to the PCC. Figure 4 shows the DSTATCOM's dynamic performance in PFC mode with the nonlinear load. Source current, compensatory current, load current, and $v_{s,a,b,c}$ are displayed in Fig. 4, along with v_{dc}. Phase a of the nonlinear load is opened between 0.4 s and 0.5 s. Supply current is observed to be reduced in amplitude between 0.4 s and 0.5 s but remain stable. The load current harmonic spectra of phase a are depicted in Fig. 5, while Fig. 6 illustrates the supply current harmonic spectra of phase a when operating under nonlinear load conditions.

As seen from Figs. 4–6, phase a load current and supply current have respective THD of 26.48% and 4.65%, so the THD value of 4.65% is within the IEEE-519 Standard limits [32]. It is evident from the characteristics of i_{sa}, i_{sb} and i_{sc} that the PNLMM-

controlled DSTATCOM effectively compensates for the distorted supply current even under the unbalanced nonlinear loading conditions. DSTATCOM assists in maintaining sinusoidal supply current and satisfactorily regulates the DC bus voltage. In the PFC mode, it also decreases harmonics under dynamic and steady-state loading conditions. Table II illustrates the compensation of individual supply current harmonics. As seen, the most dominant 5th harmonic component is reduced to 0.64 % from 17.98%, the 7th harmonic component is reduced to 0.5% from 11.78%, whereas the 11th harmonic component is reduced to 0.27 % from 5.23%. Similarly, higher order harmonic components of the 13th, 17th and 19th have all been reduced to lower values. If these dominant harmonic components are not effectively compensated, they would cause excessive heating in various loads and produce pulsating torque in AC motors connected to PCC. Figure 7 depicts the waveforms of intermediate signals of the PNLMM algorithm, incldluing the characteristics of phase a signals G_{pa}, w_{pa}, e_{pa}, w_{pavg} and σ_a.

When the load from phase a is quickly disconnected between 0.4 s and 0.5 s, the weight w_{pa}, error e_{pa}, and internal signal G_{pa} all fall to zero, as shown in Fig. 7. However, phases b and c of the load are still connected to the supply. Therefore, the weight w_{pavg} is not reduced significantly. The characteristics of w_{pa} under balanced and unbalanced loading conditions show the effective fundamental current extraction ability of the proposed control algorithm.

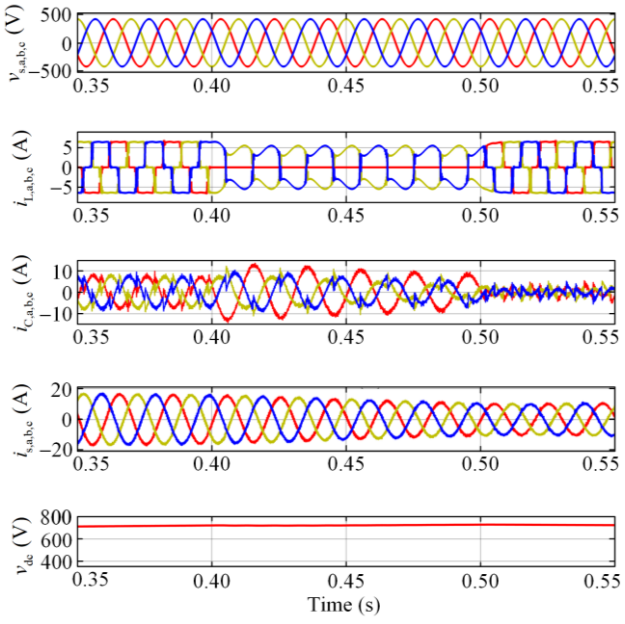

Fig. 4. Dynamic behavior of distribution static compensator when subjected to varying nonlinear load.

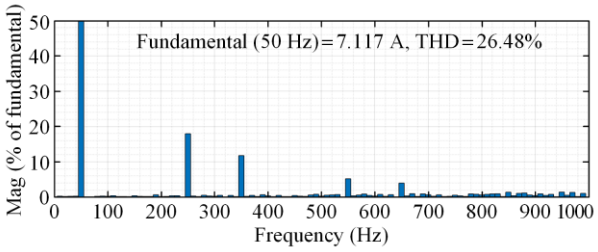

Fig. 5. Source current harmonic spectrum before compensation.

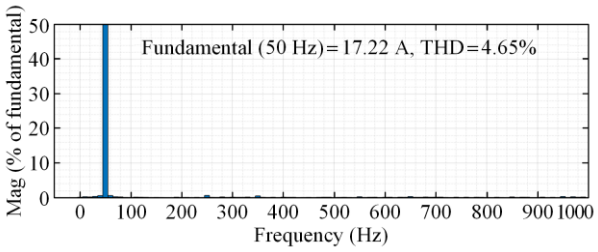

Fig. 6. Source current harmonic spectrum after compensation.

TABLE II
THD FOR SOURCE CURRENT BEFORE & AFTER COMPENSATION

Harmonic order	Harmonic currents (% of fundamental)	
	Before compensation (%)	After compensation (%)
5th	17.98	0.64
7th	11.78	0.50
11th	5.23	0.27
13th	4.01	0.32
17th	1.42	0.21
19th	1.45	0.33

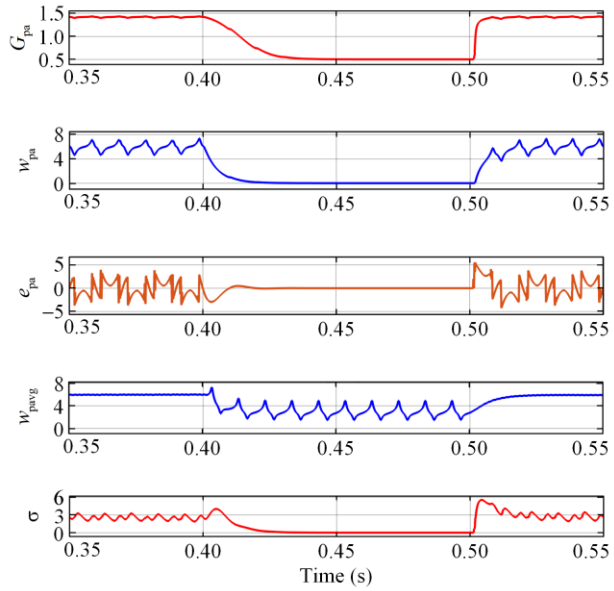

Fig. 7. Intermediate signals of PNLMM algorithm under nonlinear loading condition.

B. Load Balancing by Distribution Static Compensator Under Linear Loaded Condition

Figure 8 depicts the DSTATCOM's dynamic behaviour under unbalanced linear load conditions.

Waveforms of $v_{s,a,b,c}$, unbalanced load current, compensating current, supply current and self-sustained DC bus voltage are shown in Fig. 8. Load unbalancing is created by connecting three different linear loads ($Z_a = 40 + j20.42\ \Omega$, $Z_b = 50 + j26.70\ \Omega$ and $Z_c = 110 + j131.94\ \Omega$) in star, which results in the unbalanced three-phase current at the load side. To exacerbate the existing linear load unbalance, a deliberate omission of one load phase within a specified time interval is enacted to and its effect on the system is analyzed. The detection of neutral current imbalance is based on the variation between the reference and actual neutral currents. The mismatch between the reference and actual neutral currents provides triggering of the DSTATCOM's fourth leg IGBTs, thereby enabling the compensation of the unbalanced neutral current through appropriate switching actions.

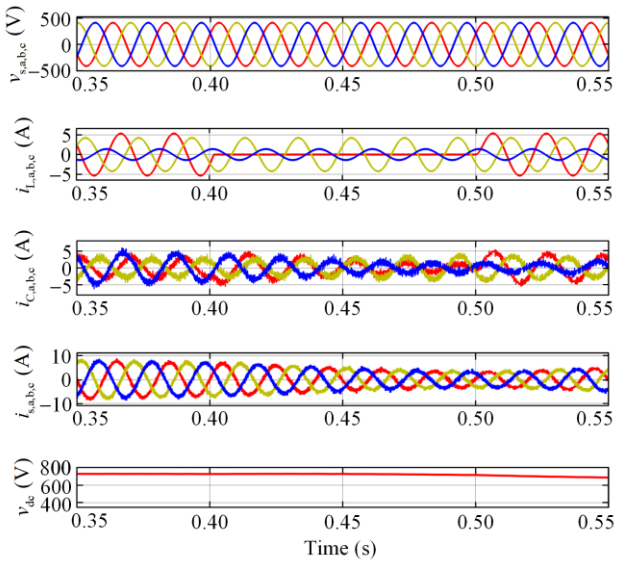

Fig. 8. Dynamic behavior of distribution static compensator when subjected to linear load.

The load from phase a has been removed from 0.4 s to 0.5 s. Even when load current is unbalanced, Fig. 8 shows balanced supply current. Figure 9 portrays the waveforms of i_{Ln}, i_{cn} and i_{sn}. As seen, the grid supplies only a fraction of the compensated neutral current (0.1 A) during unbalanced linear load conditions. The supplied neutral current remains 0.1 A even after the removal of phase a load for 0.1 s. These results are acceptable under varying unbalanced linear loads. Figure 10 depicts the internal signals of the PNLMM-based control algorithm under an unbalanced linear loaded condition when phase a is removed from a linear unbalanced three-phase load between 0.4 s and 0.5 s.

The dynamic responses of $G_{pa}(n)$, $w_{pa}(n)$, $e_{pa}(n)$, $w_{pavg}(n)$ and the internal signal $\sigma_a(n)$ shown in Fig. 10 prove that the DSTATCOM works well under the unbalanced dynamic linear load. It is observed from Fig. 10 that, at the time of phase a load removal between 0.4 s to 0.5 s, the magnitudes of $w_{pa}(n)$, $e_{pa}(n)$ and $\sigma_a(n)$ reduce to zero. However, there is only slight reductions in $G_{pa}(n)$ and $w_{pavg}(n)$ under unbalanced linear loading conditions. The various internal signals shown in Fig. 10 are different from the characteristics shown in Fig. 7. This is due to the fact that the magnitudes of load current are equal for nonlinear loading conditions, while load current magnitudes for linear loading conditions are not equal in the study. Table III shows the performance of the proposed control before and after the shunt compensation.

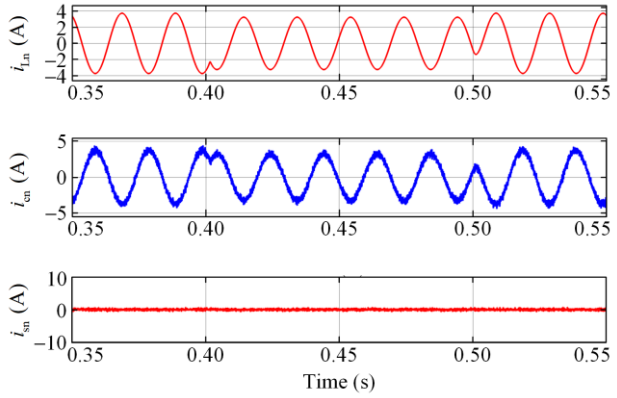

Fig. 9. Dynamic performance of distribution static compensator for neutral current compensation.

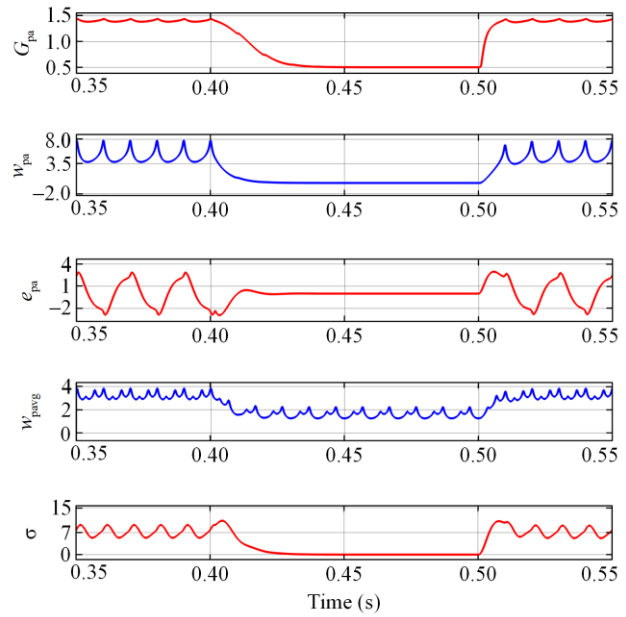

Fig. 10. Intermediate signals of PNLMM algorithm under unbalanced linear loading condition.

TABLE III
PERFORMANCE OF PROPOSED ALGORITHM BEFORE AND AFTER COMPENSATION

Performance under nonlinear loading	
Grid current THD before compensation	26.48 %
Grid current THD after compensation	4.65 %
Performance under linear loading	
Supply-side neutral current before compensation	3.74 A
Supply-side neutral current after compensation	0.1 A

C. Experimental Analysis

The study of the presented adaptive control technique is validated by experimental evaluation using real-time simulation based on the dSPACE 1202 real-time controller. The test system setup is depicted in Fig. 11. Real-time simulation is performed by building the simulator in C-code generated in the host computer. The development computer compiler is used to translate these generated codes which are embedded in C language. The Simulink model is then transferred to the dSPACE, and the test model is brought to the ControlDesk with the help of RTW. ControlDesk allows the interface in real-time-based applications, while also enables the monitoring of various signals. In ControlDesk, control signals can be switched from one state to another state using a virtual panel. Any unbalanced condition can be created using the virtual panel, and the system performance can be monitored. Monitoring of the signals is done using the Keysight DSOX1102G oscilloscope.

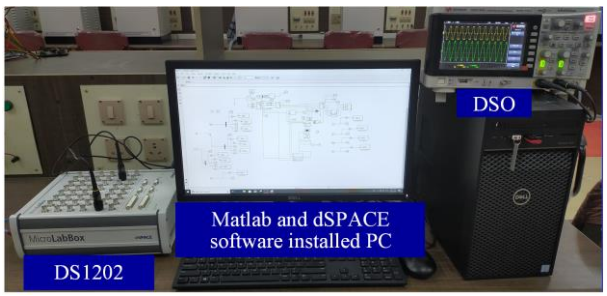

Fig. 11. Test system setup of real-time simulation.

Figures 12(a)–(h) illustrate the real-time simulation test results. Unbalanced load is introduced into the system during a real-time simulation test by removing phase a load. Figure 12(a) illustrates the waveforms of currents i_{La} and i_{Ca} for a nonlinear loading scenario. As illustrated in Fig. 12(a), the DSTATCOM compensates for distorted current generated at the PCC. Figure 12(b) illustrates the currents i_{sa} and i_{Ca}, and shows that the PNLMM-controlled DSTATCOM compensates for the distorted load current even when the unbalanced nonlinear loading condition is applied. Even with unbalanced loading, as shown in Fig. 12(c), the DC link voltage stabilizes at its rated value (700 V). Figure 12(d) shows the changes in e_{pa} with respect to i_{La}, while Fig. 12(e) shows w_{pa} signal when the load is removed. Signals e_{pa} and w_{pa} are reduced to zero if phase a is opened, which exhibits the quick response of the proposed PNLMM algorithm. Figures 12(f)–(h) depict the intermediate signals w_{pavg}, w_{sp} and w_{cp}, respectively. These intermediate signals are reduced to lower values when unbalancing is created in phase a. The signals obtained in the experimental analysis match those observed in the simulation based analysis.

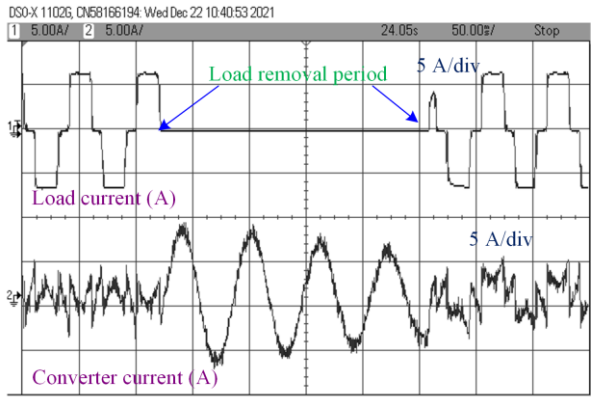

(a)

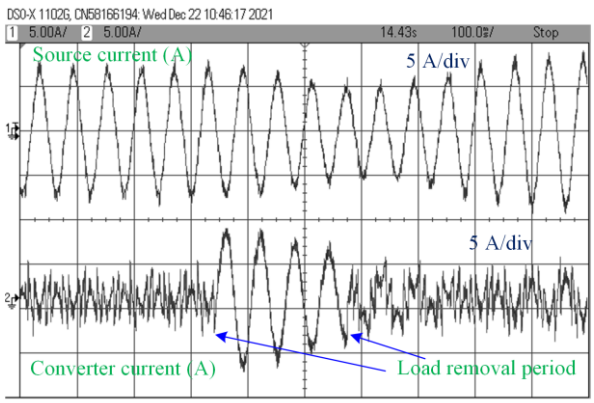

(b)

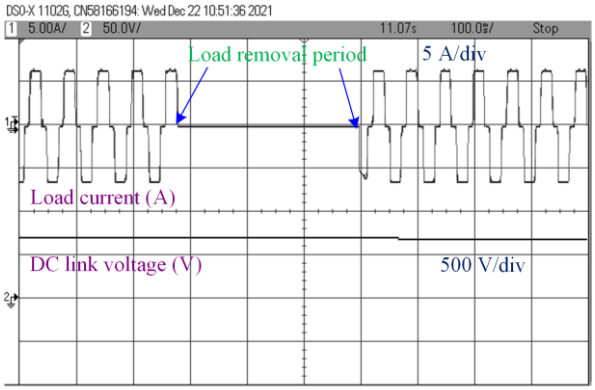

(c)

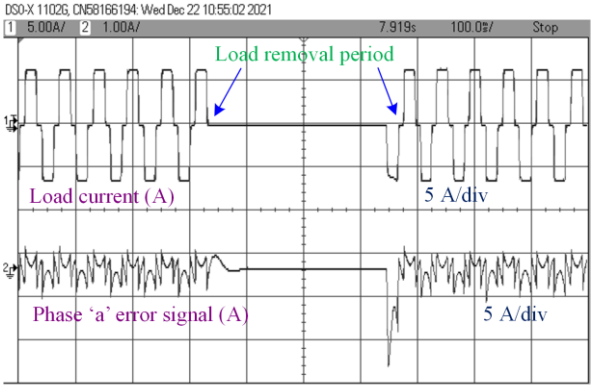

(d)

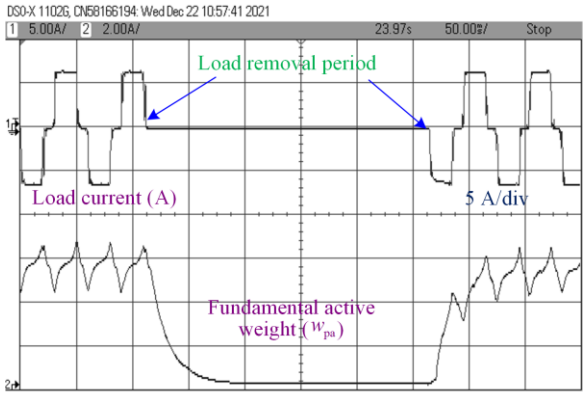

(e)

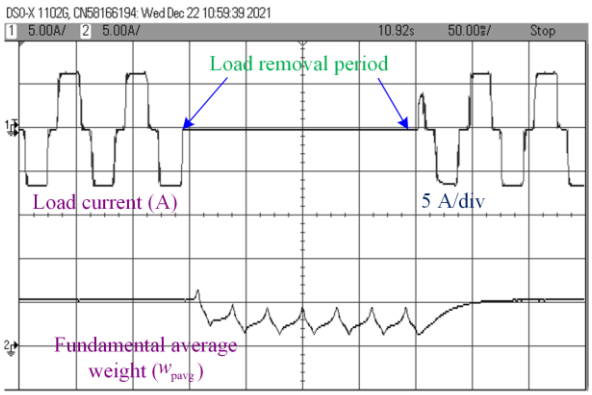

(f)

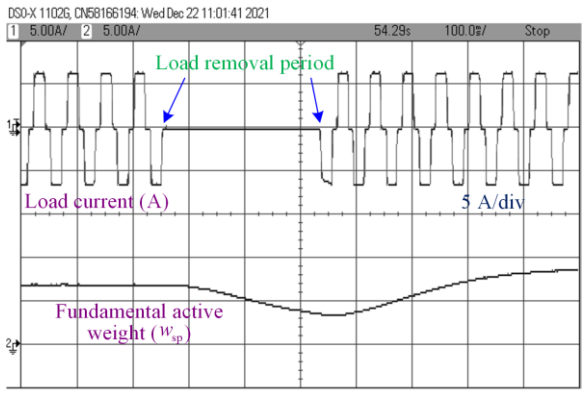

(g)

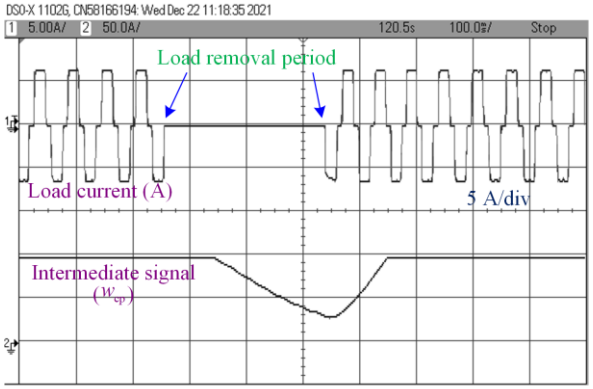

(h)

Fig. 12. Real time analysis of proposed PNLMM control. (a) Load current (i_{La}) and converter current (i_{Ca}). (b) Source current (i_{sa}) and converter current (i_{Ca}). (c) Load current (i_{La}) and DC voltage (v_{dc}). (d) Load current (i_{La}) and error signal (e_{pa}). (e) Load current (i_{La}) and (w_{pa}). (f) Load current (i_{La}) and (w_{pavg}). (g) Load current (i_{La}) and w_{sp} . (h) Load current (i_{La}) and w_{cp} .

D. Analysis of the PNLMM Control Algorithm in Comparison to other Adaptive Algorithms

The proposed PNLMM algorithm's dynamic response is compared to those of the four existing adaptive algorithms, i.e., Adaline LMS [17], LLMLF [18], PNLMF [19], and RLM [29]. Figure 13 illustrates the dynamic response of the w_{pa} . The unbalancing is introduced between 0.4 s and 0.5 s by opening phase a of the load. Observations from Fig. 13 reveal that, under balanced loading conditions, the proposed control algorithm exhibits the lowest oscillation compared to the four existing adaptive control algorithms, highlighting its robust performance. The proposed PNLMM algorithm achieves a settling time of 30 ms following the introduction of unbalanced loading created by the removal of phase a of the load.

Table IV compares the existing adaptive controls' dynamic and steady-state performance parameters with the proposed PNLMM control. As seen, the proposed PNLMM adaptive filter's convergence speed is the fastest compared to other algorithms. Compared to existing adaptive algorithms, the proposed least mean M-estimate technique also extracts the fundamental load current more accurately.

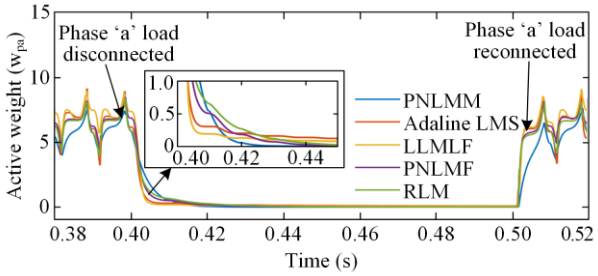

Fig. 13. Comparative analysis of the proposed filter with Adaline LMS, LLMLF, PNLMF and RLM.

TABLE IV
COMPARATIVE PERFORMANCE OF PROPOSED ALGORITHM

Algorithm	Oscillations in active weight (w_{pa} (A))	Settling time after the load unbalance (ms)	Computation burden
Adaline-LMS [17]	5.95	More than 100	Low
LLMLF [18]	4.02	More than 100	High
PNLMF [20]	4.36	50	High
RLM [29]	4.85	60	Medium
Proposed	3.6	30	Medium

IV. CONCLUSION

The presented PNLMM-based control method has been used to evaluate the effectiveness of a four-leg VSC-based distribution static compensator in reducing the impacts of nonlinear loads at PCC. Under varied loading scenarios, the proposed technique has been found to be suitable for extracting reference supply currents from non-sinusoidal and polluted load currents. The optimal value of updated filter weights has been estimated in terms of score function, which has been found suitable for filtering the impulsive noise of error signals. The performance of the proposed strategy has been analyzed by considering nonlinear and linear loads at the PCC of the distribution grid. The distorted grid current of the distribution system can be effectively compensated by the PNLMM controlled DSTATCOM and grid current THD level is reduced and complies with the IEEE-519 Standard. Moreover, reactive power compensation under unbalanced linear and nonlinear loading conditions has been demonstrated. The self-supporting DC bus voltage is regulated even for small changes in the load. The fundamental current extraction ability of the proposed PNLMM-based control algorithm is verified by comparing it with Adaline-LMS, LLMLF, PNLMF and RLM adaptive algorithms. Real-time simulation-based experimentation demonstrates the algorithm's performance and proves its effectiveness.

ACKNOWLEDGMENT

The authors would like to acknowledge the support of Renewable Energy Laboratory, School of Electrical and Electronics Engineering, SASTRA Deemed University, Thanjavur, India.

AUTHORS' CONTRIBUTIONS

Jayant Sharma: methodology, software, writing-original draft, and visualization. Chinnayan Karuppaiyah Sundarabalan: supervision, conceptualization, writing-review & editing. Chelladurai Balasundar: visualization and investigation. All authors read and approved the final manuscript.

FUNDING

This work is carried out without the support of any funding agency.

AVAILABILITY OF DATA AND MATERIALS

Not applicable.

DECLARATIONS

Competing interests: The authors declare that they have no known competing financial interests or personal relationships that could have appeared to influence the work reported in this article.

AUTHORS' INFORMATION

Jayant Sharma received the B.Eng. degree in electrical and electronics engineering from RGTU, Bhopal, India, in 2012, and the M.Tech. degree in Power electronics and drives from NIT Rourkela, India, in 2015. He joined SASTRA Deemed University, Thanjavur, Tamilnadu, India as assistant professor in 2017, where he is currently working toward the Ph.D. degree in the School of Electrical and Electronics Engineering. His fields of interest include power electronics, power quality, fuzzy logic, and design of electric vehicle charging systems.

Chinnayan Karuppaiyah Sundarabalan received his B.E. degree in electrical and electronics engineering, M.E. degree in Power Management, and Ph.D. degree in electrical engineering from Anna University, India, in 2010, 2012, and 2016, respectively. He is currently working as a senior assistant professor in the School of Electrical and Electronics Engineering at SASTRA Deemed University, Thanjavur, Tamilnadu, India. He received Technical Education Quality Improvement Programme (TEQIP) research fellowship for his doctoral studies. He is receipient of the IEEE MAS Best Publication Award 2024. He is a member of IEEE Intelligent Transportation Society, IEEE Vehicular Technology Society, and IEEE Industrial Electronics Society. He is serving as an associate editor in the *IEEE Transactions on Intelligent Transportation Systems*. Also, he serves as a reviewer for various IEEE journals such as IEEE Transactions on Industrial Electronics, IEEE Transactions on Industrial Informatics, IEEE Transactions on Energy Conversion, etc. His research interests include power quality, electric vehicles, electric vehicle charging circuits, distribution grid impacts and intelligent controllers.

Chelladurai Balasundar received the B.E. degree in EEE from Anna University, in 2012, and the M.E. degree in Electrical Drives and Embedded Control from Anna University, in 2015. He received the Ph.D. degree in the specialisation of electric vehicle battery charger and grid integration from the School of EEE at SASTRA Deemed University, Thanjavur. Also, he

received the Founder Chancellor's award for the best Ph.D. dissertation in SASTRA Deemed University. Currently, he is working as an assistant professor in the Department of EEE, Thiagarajar College of Engineering, Madurai, Tamilnadu, India. He serves as a reviewer for various IEEE Transactions and other reputed journals. His fields of interest include power electronics, power quality, fuzzy logic, and the design of electric vehicle charging systems.

REFERENCES

[1] S. K. Bilgundi, R Sachin, and H. Pradeepa *et al*., "Grid power quality enhancement using an ANFIS optimized PI controller for DG," *Protection and Control of Modern Power Systems*, vol. 7, no. 1, pp. 1-14, Jan. 2022.

[2] R. T. Hock, Y. R. de Novaes, and A. L. Batschauer, "A voltage regulator for power quality improvement in low-voltage distribution grids," *IEEE Transactions on Power Electronics*, vol. 33, no. 3, pp. 2050-2060, Mar. 2018.

[3] B. Singh, V. Jain, and Seema A *et al*., "Power quality improvement in a PV based EV charging station interfaced with three phase grid," in *IECON 2021-47th Annual Conference of the IEEE Industrial Electronics Society*, Toronto, Canada, Oct. 2021, pp. 1-6.

[4] M. Pushkarna, H. Ashfaq, and R. Singh *et al*., "Power quality problems due to upgrades in the power system with RES and front-line solutions," in *2022 2nd International Conference on Power Electronics & IoT Applications in Renewable Energy and its Control (PARC)*, Mathura, India, Jan. 2022, pp. 1-6.

[5] A. Benslimane, J. Bouchnaif, and M. Essoufi *et al*., "Comparative study of semiconductor power losses between CSI-based STATCOM and VSI-based STATCOM, both used for unbalance compensation," *Protection and Control of Modern Power Systems*, vol. 5, no. 1, pp. 1-14, Jan. 2020.

[6] D. Çelik and H. Ahmed, "Enhanced control of superconducting magnetic energy storage integrated UPQC for power quality improvement in EV charging station," *Journal of Energy Storage*, vol. 62, 2023.

[7] O. J. K. Oghorada, L. Zhang, and H. Han *et al*., "Inter-cluster voltage balancing control of a delta connected modular multilevel cascaded converter under unbalanced grid voltage," *Protection and Control of Modern Power Systems*, vol. 6, no. 3, pp. 1-11, Jul. 2021.

[8] P. Shadangi, S. D. Swain, and P. K. Ray *et al*., "Experimental verification of DSTATCOM for various non-linear load," *International Journal of Emerging Electric Power Systems*, vol. 23, no. 5, pp. 683-690, May 2022.

[9] Y. Zhao, A. An, and Y. Xu *et al*., "Model predictive control of grid-connected PV power generation system considering optimal MPPT control of PV modules," *Protection and Control of Modern Power Systems*, vol. 6, no. 4, pp. 1-12, Oct. 2021.

[10] H. A. Khalid, C. Cecati, and N. A. Al-Emadi *et al*., "Differential flatness-based performance enhancement of a vector controlled VSC with an LCL-filter for weak grids," *IEEE Access*, vol. 9, pp. 33557-33568, 2021.

[11] H. A. Khalid, N.A. Al-Emadi, and L. Ben-Brahim *et al*., "A novel control scheme for three-phase seven-level packed U-cell based DSTATCOM", *Electric Power System Research*, vol. 182, 2020.

[12] S. Chakraborty, S. Mukhopadhyay, and S. K. Biswas, "Coordination of D-STATCOM & SVC for dynamic VAR compensation and voltage stabilization of an AC grid interconnected to a DC microgrid," *IEEE Transactions on Industry Applications*, vol. 58, pp. 634-644, Jan.-Feb. 2022.

[13] D. Çelik, "Lyapunov based harmonic compensation and charging with three phase shunt active power filter in electrical vehicle applications," *International Journal of Electrical Power & Energy Systems*, vol. 136, 2022.

[14] G. S. Chawda, A. G. Shaik, and O. P. Mahela *et al*., "Performance improvement of weak grid-connected wind energy system using FLSRF-controlled DSTATCOM," *IEEE Transactions on Industrial Electronics*, vol. 70, no. 2, pp. 1565-1575, Feb. 2023.

[15] T. S. Saradhisatwik, Gankidinishma, and U. Hemanthchandra *et al*., "Power quality improvement in solar powered standalone system using D-STATCOM," in *4th International Conference on Smart Systems and Inventive Technology (ICSSIT)*, Tirunelveli, India, Jan. 2022.

[16] J. Zhang and K. Liu, "Harmonic detection for three-phase circuit based on the improved analog LMS algorithm," in *International Conference on Electrical Machines and Systems"*, Wuhan, China, Oct. 2008.

[17] G. S. Chawda and A. G. Shaik, "Enhancement of wind energy penetration levels in rural grid using ADALINE-LMS controlled distribution static compensator," *IEEE Transactions on Sustainable Energy*, vol. 13, no. 1, pp. 135-145, Jan. 2022.

[18] N. Kumar, B. Singh, and B. K. Panigrahi, "LLMLF-based control approach and lpo mppt technique for improving performance of a multifunctional three-phase two-stage grid integrated PV system," *IEEE Transactions on Sustainable Energy*, vol. 11, no. 1, pp. 371-380, Jan. 2020.

[19] M. Badoni, A. Singh, and A. K. Singh *et al*., "Grid tied solar PV system with power quality enhancement using adaptive generalized maximum versoria criterion," *CSEE Journal of Power and Energy Systems*, vol. 9, no. 2, pp. 722-732, Mar. 2023.

[20] D. Jaraniya, U. Gupta, and S. Kumar *et al*., "Multifunctional bidirectional charging system for EVs and grid with improved power quality using a sparse proportionate-NLMF based method," *CSEE Journal of Power*

and Energy Systems, vol. 9, no. 3, pp. 1203-1213, May 2023.

[21] P. Shah and B. Singh, "Adaptive observer based control for rooftop solar PV system," in *IEEE Transactions on Power Electronics*, vol. 35, no. 9, pp. 9402-9415, Sept. 2020.

[22] B. Chelladurai, C. K. Sundarabalan, and S. N. Santhanam *et al*., "Interval type-2 fuzzy logic controlled shunt converter coupled novel high-quality charging scheme for electric vehicles," *IEEE Transactions on Industrial Informatics*, vol. 17, no. 9, pp. 6084-6093, Sept. 2021.

[23] C. Balasundar, C. K. Sundarabalan, and N. S. Srinath *et al*., "Interval type2 fuzzy logic-based power sharing strategy for hybrid energy storage system in solar powered charging station," *IEEE Transactions on Vehicular Technology*, vol. 70, no. 12, pp. 12450-12461, Dec. 2021.

[24] E. Hashemzadeh, M. Khederzadeh, and M. R. Aghamohammadi *et al*., "A robust control for D-STATCOM under variations of DC-link capacitance," *IEEE Transactions on Power Electronics*, vol. 36, no. 7, pp. 8325-8333, Jul. 2021.

[25] A. M. Saif, M. Tinari, and P. Ciammaichella *et al*., "Backstepping control for multilevel STATCOM," in *IEEE Energy Conversion Congress and Exposition (ECCE)*, Detroit, MI, USA, Oct. 2020.

[26] M. Badoni, A. Singh, and B. Singh, "Power quality enhancement using Euclidean direction search based control technique," *IEEE Transactions on Industrial Electronics*, vol. 67, no. 3, pp. 2231-2240, Mar. 2020.

[27] S. Das, D. Chatterjee, and S. K. Goswami, "A reactive power compensation scheme for unbalanced four-wire system using virtual Y-TCR model," *IEEE Transactions Industrial Electronics*, vol. 65, pp. 3210-3219, Apr. 2018.

[28] Z. Bai, Y. Pang, and Z. Xiang *et al*., "A capacitive-coupling winding tap injection DSTATCOM integrated with distribution transformer for balance and unbalance operations," *IEEE Transactions on Industrial Electronics*, vol. 70, no. 2, pp. 1081-1093, Feb. 2023.

[29] Y. Zou, S. C. Chan, and T. S. Ng, "A recursive least M-estimate (RLM) adaptive filter for robust filtering in impulse noise," *IEEE Signal Processing Letters*, vol. 7, no. 11, pp. 324-326, Nov. 2000.

[30] Y. Zou, S. C. Chan, and T. S. Ng, "Least mean M-estimate algorithms for robust adaptive filtering in impulse noise," *IEEE Transactions on Circuits and Systems II: Analog and Digital Signal Processing*, vol. 47, no. 12, pp. 1564-1569, Dec. 2000.

[31] Z. Zheng, Z. Liu, and J. Zhao, "Bias-compensated sparsity-aware NLMM algorithms for robust adaptive echo cancellation," *IEEE Transactions on Circuits and Systems I: Regular Papers*, vol. 67, pp. 2383-2396, 2020.

[32] IEEE Recommended Practice and Requirements for Harmonic Control in Electric Power Systems, IEEE Std 519-2014 (Revision of IEEE Std 519-1992), 2014.